EXPLORING THE ROLE OF SINGLE NUCLEOTIDE POLYMORPHISMS IN VARICELLA ZOSTER VIRUS VACCINE ATTENUATION IN SKIN

Elizabeth Da-Yong Lee

A Thesis in the

Department of Microbiology & Immunology

Submitted in partial fulfillment of the requirements for the degree of Master of Science in the College of Graduate Studies of State University of New York, Upstate Medical University.

Approved Jennifer Moffat
(Sponsor's signature)

Date May 28, 2024

ABSTRACT

Elizabeth Da-Yong Lee: Exploring the Role of Single Nucleotide Polymorphisms in Varicella Zoster Virus Vaccine Attenuation in Skin
(Under the direction of Jennifer Moffat)

Varicella zoster virus (VZV) is a disease that can be detrimental to the health of children in its primary form, chicken pox, and later in the elderly as its reactivated form, shingles. Before the advent of the vaccine, Varivax, VZV was endemic in the United States as it is highly contagious and can be spread through both direct contact and aerosol particles. Varivax, or vOka, is a live attenuated vaccine, and while effective, has side effects ranging from rashes to possible VZV reactivation. While the vaccine has reduced the incidence and severity of VZV, there is still little known about the mechanism of its attenuation in skin. vOka is genetically heterogeneous with hundreds of single nucleotide polymorphisms (SNPs) that are a mixture of wild-type and vOka nucleotides. Previous studies have demonstrated the key to attenuation may be through five SNPs in the open reading frame (ORF) 62 region found to be fixed and stable across different licensed vOka preparations around the world. ORF62 contains the gene for IE62, a transactivator protein responsible for regulating the expression of viral genes and the host gene for KRT15, a cytokeratin protein. This project focused on if two SNPs, located in the loci positions 106262 and

107252, that are found to be almost 100% conserved across all variations of vOka are responsible for the attenuation in human skin and induction of KRT15.

We evaluated four mutant viruses with SNPs found in vOka and discovered that a double SNP mutation stunted virus growth in HFF cells. In addition, we found no significant difference in the growth of our viruses in skin but variability in successful infection. Furthermore, in infected skin, we found that VZV-ORF57-Luc and single mutant virus, 68-958, upregulate KRT15 expression with VZV infection while single mutant virus, 68-62S-A, may downregulate KRT15 expression with VZV infection. This project is important because it may reveal the molecular basis of attenuation of the licensed varicella vaccine. This information could be used to make a vaccine that contains only the attenuated genotype.

ACKNOWLEDGEMENTS

I would like to thank my advisor, Dr. Jennifer Moffat, for her help and support throughout this past year. Dr. Moffat's guidance and wisdom were crucial for navigating this program. I would also like to thank the members of the Moffat lab, specifically Dr. Megan Lloyd, whose training and support were invaluable. In addition, I would like to thank the members of my thesis committee, Drs. Eain Murphy and Paul (Kip) Kinchington, for challenging me whilst providing unending guidance, suggestions, and support during my thesis work. I would also like to thank Dr. Nathan Roy for his instructions and advice about microscopy, immunohistochemistry staining, and life. I would like to extend a thanks to my program advisor, Dr. Evelyn Voura, for her support and mentorship. In addition, I would like to thank the current members of the Department of Microbiology and Immunology for the great friendships and cherished memories they have provided me with. I would also like to thank my friends for their continued check-ins and support even whilst busy with their own programs and lives. Most importantly, I would like to thank my parents, Jongwon and Meeheun, and my younger sister, Esther, for all the love, support, reassurance, and patience they have consistently provided me. I could not have completed this program without my massive support network, and I am truly grateful to each one of you. Thank you.

TABLE OF CONTENTS

LIST OF FIGURES

LIST OF ABBREVIATIONS

ARPE-19	Human Retinal Pigment Epithelial
CPE	Cytopathic Effect
DDR	DNA Damage Response
DPI	Days Post Infection
gE	Glycoprotein E
GPEF	Guinea Pig Embryo Fibroblast
HEK	Human Epidermal Keratinocyte
HFF	Human Foreskin Fibroblast
HZ	Herpes Zoster
IE	Immediate Early
KRT15	Cytokeratin 15
ORF	Open Reading Frame
SCID-hu	Severe Combined Immunodeficiency
SNP	Single Nucleotide Polymorphism
SOC	Skin Organ Culture
VZV	Varicella Zoster Virus
WT	Wild-Type

INTRODUCTION

Varicella Zoster Virus (VZV) is a double-stranded DNA virus that is part of the alphaherpesviridae family.[1] The primary form of infection varicella, also colloquially known as chickenpox, is characterized by fever, malaise, and fluid-filled blisters surrounded by an erythematous base described as "dew drops on a rose petal."[1] It is highly contagious and spreads by aerosol transmission or direct contact with a lesion of an infected individual.[1] Varicella is seen mostly in children, with symptoms demonstrating high penetrance unlike other herpes viruses that often remain asymptomatic in immunocompetent hosts.[1] Upon exposure, VZV establishes primary infection by entering a host body through the mucosal epithelial cells of the upper respiratory tract.[1] The mucosal epithelial cells line the crypts of lymphoid tissue where VZV will replicate and infect lymphocytes and immune presenting cells.[1] CD4+, CD8+, and CD4+/CD8+ T cells were specifically demonstrated to be permissive in a previous study where severe combined immunodeficiency (SCID-hu) mice with human T cell xenografts were infected with VZV.[1] These infected T cells travel through the bloodstream to extravasate and home in on epidermal keratinocytes where VZV can replicate and begin the process of skin infection.[2] This entire process accounts for the incubation period of VZV primary infection that occurs over 10-21 days.[3] During the primary infection process, virions can access the sensory ganglia via T cell or retrograde axonal transport from skin to establish latency in the cell bodies.[3,4] Latent VZV can reactivate to cause herpes zoster (HZ), also known as shingles, in the elderly and/or immunocompromised. Zoster is characterized by a painful, dermatomal vesicular rash that is unilateral – specific to the dermatome that is affiliated with the infected ganglia.[3,4]

Around 25-35% of individuals experience reactivation in a lifetime, with the severity and complications increasing with age.[4] Post-shingles complications can be severe including post herpetic neuralgia, meningoencephalitis, and cranial nerve palsies.[4] While varicella is oftentimes a self-limiting disease in immunocompetent hosts, reactivated zoster can be deadly in the same host years later. Although there are antiviral treatments such as acyclic guanosine analogs, like acyclovir, available to both varicella and zoster patients, preventing VZV disease even if infection still occurs is important.[5]

A live attenuated vaccine, vOka, for VZV exists in the United States and is effective in reducing both primary (Varivax®) and reactivated (Zostavax®) diseases.[6] The parent strain, pOka, was first isolated from the blister fluid of a Japanese child with chickenpox from wild-type (WT) VZV in 1971.[6] vOka was derived through serial passages of pOka in human embryonic lung cells, guinea pig embryo fibroblasts (GPEF), and human fibroblasts. The adaptations vOka made in these cells resulted in attenuation and a loss of virulence.[7] Before the advent and licensure of the vaccine in the United States in 1995, approximately 4 million cases of varicella were reported every year with an average of 11,000 hospitalizations and 100 deaths.[8] A study during the four-year period after licensure and distribution of the vaccine found cases of varicella declined by over 80%, and VZV-associated hospitalizations and mortality have both also decreased dramatically by 88% and 60%, respectively.[8,9] While vOka has reduced the disease burden of varicella and zoster in the population, the vaccine has rare side effects including rash, transmission, and reactivation – all similar to the behavior of WT VZV but at a lesser severity.[7,10] Particularly, latent vOka can reactivate as herpes zoster which is indistinguishable from WT VZV in both healthy and immunocompromised hosts.[10] In a

10-year review of post zoster vaccination side effects, while the majority of recipients reported non-serious symptoms (93%), the 7% that reported serious syndromes included symptoms of HZ necrotizing retinitis, ophthalmic HZ, and disseminated HZ that had led to one fatal outcome.[11] While the percentage of side effects seems rare, 7% of the 23,556 individuals that were a part of this study is around 1,650 affected with serious symptoms of this vaccination.[11] Addressing these side effects is difficult because the molecular basis of attenuation in vOka is not well understood.[7]

As a human-specific virus, VZV is difficult to study with classic animal models.[7] It is believed that during the multiple passages from pOka, vOka attenuation was derived via mutations in the genome to adapt and grow in GPEFs.[7] Studying vOka proves further difficult because it is genetically heterogeneous with 200-300 single nucleotide polymorphisms (SNPs) that are a mixture of the wild-type and vOka nucleotides.[7,12] In addition, vOka strains from different vaccine manufacturers have genetic variations, most likely due to the differences in production methods and the number of additional passages in cells.[12] Of the hundreds of SNPs seen across vOka genomes, there are 137 "core" SNPs seen consistently and six core SNPs near fixed and stable across all vOka preparations.[7] Five of the six SNPs are located in the same open reading frame (ORF), ORF62 and ORF71, and have long been thought to be a possible mechanism for attenuation.[6] ORF62 and ORF71 are diploid genes that are located in the internal repeat short and terminal repeat short regions of the unique short segments in the genome, respectively, and encode for immediate early (IE) protein, IE62.[13] IE62 is a large protein that is packaged in the viral tegument and acts as a major VZV transactivator for early and late proteins. It is essential and plays a critical part in VZV replication.[14–16]

During the lytic phase of infection, VZV expresses all 71 of its ORFs beginning with immediate-early (IE), followed by early (E), and ending with late (L).[17] While the lytic phase of infection has been elucidated, the latent phase of VZV is under study as it is difficult to get an accurate idea of viral gene transcription because human ganglia must be collected post-mortem due to the nature of VZV latency in neurons. In previous studies, viral gene expression studied 24 hours post-mortem may have been too late after death to get an accurate landscape because of post-mortem release of repression.[18] In more recent studies, RNA-seq analyses of VZV transcripts taken 6 hours post-mortem found ORF63 and a novel spliced latency-associated VZV transcript (VLT) found to be antisense to gene 61. Another study looked at four ganglionic samples and confirmed ORF63 to be found in all four samples while there was variation in other ORF transcripts, including ORF62.[17,18] A recent study by Sadaoka et al. found that another SNP in ORF31 that encodes for glycoprotein B, a VZV envelope protein important for virus fusion and infection of neurons, was maintained in vOka and may also contribute to attenuation.[7] The results of this study suggest that while ORF62 has long been suspected as the key to attenuation, there may be other contributions that decrease the likeliness of virulence reversion.[8]

A possible mechanism for IE62 affecting attenuation of vOka is via control of KRT15 expression. KRT15, or cytokeratin 15, is a type 1 cytokeratin protein that acts as a putative marker for human epidermal stem cells found in the bulge of hair follicles and basal layer of the epidermis.[19–21] Keratinocytes that expressed KRT15 are less differentiated and can also be found in the suprabasal layer of the epidermis in both normal and diseased tissues.[19] In addition, KRT15 is expressed in cells that are

proliferating in response to wound injury.[22] There has been evidence that wild-type VZV may upregulate KRT15 expression in a differentiating human epidermal keratinocyte (HEK) model.[23] Unpublished, preliminary studies demonstrate KRT15-knockout HEK lines were unable to support wild-type VZV growth. Additional preliminary studies with lentivirus transduced HEKs demonstrated that IE62, specifically, was the VZV regulatory gene that induced KRT15 expression. Through a subsequent study, KRT15 was expressed via pOka IE62 and not vOka IE62. A similar phenomenon was observed in our human skin model. Skin that was infected with wild-type VZV had abnormal upregulation of KRT15 expression.

KRT15 may be connected to the VZV DNA damage response (DDR), a cellular response to DNA damage. The DDR includes cell cycle delay or arrest, induction of cellular or DNA repairs, and, if necessary, apoptosis induction.[24] Cells sense DNA damage and induce kinases that phosphorylate downstream proteins involved in the DDR – one such protein is H2AX.[25] H2AX is a histone protein that regulates transcription and is phosphorylated to form γ-H2AX at sites of DNA damage for DNA repair and chromatin remodeling proteins to accumulate.[26] VZV infection induces the phosphorylation of H2AX in fibroblasts.[25] In preliminary studies, HEK cell lines with knockout KRT15 was exposed to ionizing radiation to induce DNA damage and γ-H2AX was quantified. Knockout KRT15 cells had decreased γ-H2AX, demonstrating a possible relationship between KRT15 levels and control of proviral aspects of the DDR. Additionally, the knockout KRT15 HEKs did not support VZV replication. Interestingly, the attenuated vOka can be induced to replicate by overexpression of KRT15 and DNA damage induction.

Our hypothesis is that the SNPs found in ORF62 are responsible for the attenuation of vOka in the skin through the regulation of KRT15 expression. Specifically, the SNPs located in the loci positions 106262 and 107252, which are conserved in Varivax at 100% and 98.7%, respectively, as compared to pOka.[6] Within the 5 conserved SNPs found in ORF62, two are in non-coding regions, one is a synonymous amino acid change, and two are non-synonymous amino acid changes.[6] We studied the non-synonymous amino acid changes. The first is in the amino acid position 628 (location 107252) that changes a polar serine into a neutral glycine. The second is in the amino acid position 958 (location 106262) that changes a positively charged arginine to a neutral glycine.[6] This position is particularly important because it is conserved 100% in all variations of vOka and is often used to distinguish vOka from wild-type VZV.[12]

MATERIALS AND METHODS

2.1 Cells

Two cell lines were used for experiments – human foreskin fibroblasts (HFF) (CCD-1137Sk; American Type Culture Collection (ATCC), Manassas, VA, USA), a primary cell line, and human retinal pigment epithelial (ARPE-19) (CRL-2302; ATCC) cells, an immortal cell line. MeWo cells, a melanoma cell line, were not used in this study because they are transformed, and their cell cycle is dysregulated. HFF cells were passaged up to a maximum of 16 times for any given experiment while ARPE-19 cells were passaged indefinitely. All cells were grown in Dulbecco's Modified Eagle Medium (DMEM 1X, Corning, Manassas, VA, USA) with 4.5 g/L glucose, L-glutamine, and sodium pyruvate and added 10% heat-inactivated fetal bovine serum (Benchmark FBS; Gemini Bio Products, West Sacramento, CA, USA), amphotericin B (250 µg/mL), and penicillin-streptomycin (5000 IU/mL). Cell cultures were incubated at 37°C in humidified 5% CO_2. Cells were split at 90-100% confluency using 0.25% 1X Trypsin-EDTA (25200056; Thermo Fischer).

2.2 Viruses

Recombinant mutant viruses were created via BAC constructs and provided by Dr. Paul Kinchington. vOka was cultured from a vial of Zostavax. Viruses used for both cell and skin organ culture experiments were maintained and passaged in HFF cells and remained cell-associated for use in experiments. Viruses are stored as 1 mL aliquots with 10% DMSO in the -80°C. Viruses are stored at around 90% infection rate, measured by cytopathic effects (CPE). Viruses used include: VZV-ORF57-Luc, vOka, 62D_v1, 62D_v3, 68-62S-A, 68-958.

Virus	Mutation	Stock Titer (via TCID50, in PFU/mL)
VZV-ORF57-Luc	ORF57 – T2A – Luciferase	4.30×10^5
vOka	Vaccine strain	4.60×10^5
62D_v1	Double mutations by order: (1) R958G (2) S628G	7.80×10^5
62D_v3	Double mutations by order: (1) S628G (2) R958G	5.40×10^3
68-62S-A	Single mutation: (1) S628G	4.80×10^4
68-958	Single mutation: (1) R958G	5.40×10^4

Table 1. List of Viruses

2.3 Luciferase Reporter

The viruses used in this project contain a luciferase gene inserted downstream of the ORF57 region separated by a self-cleaving T2A peptide. ORF57 is a kinetically late promoter that drives the expression of luciferase to reflect viral replication. Therefore, using this reporter we can track virus spread using bioluminescence imaging. The viruses express luciferase and emit light once incubated with D-luciferin (300 µg/mL in PBS; Xeno-Light™ D-Luciferin Potassium Salt, Perkin Elmer, Waltham, MA, USA) The viruses that contain the luciferase reporter are: VZV-ORF57-Luc, 62D_v1, 62D_v3, 68-62S-A, 68-958.

2.4 Virus Titer

In the past, viral titer was calculated by counting plaques in cell monolayers stained with crystal violet. Unfortunately, this method was tricky because the plaques were not always obvious nor the staining consistent. An effort was made to find an easier, faster, and more accurate method. We explored using an automated microplate reader, the BioTek Cytation 5, to detect single cell infection 24 hours after inoculation. The viruses did not express fluorescent reporters, so antibody retrieval methods with Anti-VZV (MAB8612; Sigma-Aldrich) or human IgG Isotype Control (AB_2337043; Jackson ImmunoResearch) antibodies were used to detect infected cells. Anti-VZV antibody was the best method, but detecting single cell infection was both difficult and expensive. The Cytation 5 approach was not useful for this project. Instead, the TCID50 assay was used to determine the titer, and this was the method used moving forward.

TCID50 Assay: 96-well plates were seeded with a HFF cell suspension of 2 x 10^5 cells/mL and left to incubate overnight at 37^{o}C. Once HFF cells reached 90-95% confluency, a dilution series of the virus was made in a deep well 96-well plate starting from a 10^{-1} dilution in the first row and ending with a 10^{-8} dilution in the last row. Virus dilution from the deep well 96-well plate was added to the normal HFF-seeded 96-well plate. Plates were incubated for 4-6 days for plaque formation. Plaques were detected in one of three ways. The first was via brightfield microscopy. While this method could be done with all viruses, it required a longer incubation period for plaques to be visible. The second method was immunofluorescence staining with anti-VZV. 96-well plates were washed with PBS and then fixed with 3.7% formalin in PBS for 15-20 minutes at room temperature. Plates were PBS washed, then permeabilized and blocked with a buffer solution composed of PBS-Tween (PBS-T), 1% bovine serum albumin (BSA), and 0.5%

triton for 30 minutes in the 37°C incubator. Plates were PBS washed then stained with 1:200 dilution of primary antibody, Anti-VZV, in a buffer solution (PBS-T, 1% BSA, 0.5% triton) for 1-2 hours at room temperature. Plates were PBS washed then stained with 1:2000 dilution of secondary antibody, AlexaFluor 568 (#A-11004; Invitrogen), and DAPI in a buffer solution (PBS-T, 1% BSA, 0.5% triton) for 30 minutes to 2 hours at room temperature, protected from the light. Plates were washed with PBS and read under a fluorescent microscope. This method could be done with all viruses, but it was an expensive method and usually reserved for determining with high accuracy and/or confirming stock titers. The third method was using the Xenogen IVIS™ 50. This was an easy and accurate way of checking for plaque formation but only for viruses that express luciferase. Plates were PBS washed. D-luciferin (300 µg/mL in PBS; Xeno-Light™ D-Luciferin Potassium Salt, Perkin Elmer, Waltham, MA, USA) was prepared. D-luciferin was added to the plate and incubated for 20 minutes. Plates were scanned in the IVIS™ 50. This method was used in conjunction with brightfield microscopy to ensure accurate measurements.

2.5 Growth Kinetics in Cells

Growth curves were generated in both HFF and ARPE-19 seeded 6-well plates. Cells were grown to confluence and were infected with cell-associated virus grown in HFFs. Measurements were taken daily from three wells (N=3). Measurements were taken one of two ways depending on luciferase expression ability. With luciferase expressing viruses, virus spread was measured through bioluminescence imaging. Media was removed, D-luciferin (300 µg/mL in PBS; Xeno-Light™ D-Luciferin Potassium Salt, Perkin Elmer, Waltham, MA, USA) was added, and plates were incubated for 20 minutes.

Bioluminescent signaling has been shown to correlate with viral spread.[27] In luciferase-expressing viruses, measurements began with a 6-8 hours post-inoculation value (DPI 0) and then monitored for 7 days, with measurements taken from three wells (N=3) and averaged every day. Medium was replaced after imaging. For non-luciferase-expressing viruses, virus-infected cells were harvested from three wells (N=3) every day and measured via TCID50 assays and averaged to determine virus yield.

2.6 Skin Organ Culture

Skin from breast tissue was obtained from consenting adults who were undergoing reduction mammoplasty surgeries by plastic surgeon, Dr. Gregory Baum, at SUNY Upstate Medical University in Syracuse, NY. Skin was obtained and prepared on the same day of surgery. The virus inoculum was cell-associated and grown in HFFs. Media used was DMEM with added 4% heat-inactivated FBS, amphotericin B (250 g/mL), and penicillin-streptomycin (5000 IU/mL) for skin and DMEM with added 10% heat-inactivated FBS, amphotericin B (250 g/mL), and penicillin-streptomycin (5000 IU/mL) for cells. Originally, the skin pieces were inoculated via scarification, a process where a needle was used to scratch the surface of the skin and cell-associated virus placed on top. While this was effective, it wounded the skin and could activate KRT15, skewing our results. To address this issue, we used a dermaroller and found it was conducive to infection without wound injury leading to KRT15 activation. Skin was prepared by disinfecting with both povidone iodine and ethanol first and then washed in 4% FBS DMEM. A thin layer was stripped from the top of the skin using a Weck knife and Goulian Guard (0.028”). These strips were dermarolled multiple times before being cut into 0.5 x 0.5 cm^2 pieces. To ensure a robust delivery of virus, skin pieces were placed

individually in the wells of a 48-well plate, submerged in the viral suspension, and incubated in 35°C for 2-3 hours to inoculate. Inoculated skin pieces were placed on NetWell inserts in a 12-well plate with fresh DMEM with 4% serum and incubated at 35°C. To image, skin pieces were placed in a black 24-well plate with D-luciferin (300 µg/mL in PBS; Xeno-Light™ D-Luciferin Potassium Salt, Perkin Elmer, Waltham, MA, USA) and incubated for 40 minutes before being imaged via IVIS™ 50. Skin pieces were scanned and replaced on the same NetWell inserts with fresh medium on days 1, 3, 5, 7, 10, and 14. Uninfected, dermarolled skin, day 1 virus-inoculated skin, and day 14 virus-inoculated skin pieces were collected and stored in 4% paraformaldehyde (PFA) at 4°C.

2.7 Statistical Analysis

Graphs were made using GraphPad Prism (Graph-Pad Software, San Diego, CA). Calculations were done via the GraphPad software. All data was analyzed using either Ordinary one-way ANOVA Tukey's Multiple Comparison post hoc test or an unpaired Student's t-test. A $p \leq 0.05$ was considered statistically significant.

2.8 Immunofluorescence Microscopy

Fixed skin pieces were shipped to HistoWiz for sectioning and H&E staining. Unstained sections mounted on slides were shipped back to us. These slides were deparaffinized and rehydrated: Slides were (1), submerged in xylene for 15 minutes; (2), three times in a 1:1 xylene:100% EtOH solution for 3 minutes; (3), in 100% EtOH for 3 minutes; (4), in 95% EtOH for 3 minutes; (5), in 70% EtOH for 3 minutes; (6), in 50% EtOH for 3 minutes; and (7), in DI water for 5 minutes. Slides were submerged in Antigen Unmasking Solution, Citrate-Based (H-3300-250; Vector Labs) and microwaved to boiling for 10

minutes. Once boiling, slides were placed on ice to cool to 50°C. Once cooled, slides were placed back in the microwave and boiled again for 3 minutes. Once boiling, slides were placed on ice to cool to room temperature. Once cooled, boxes were drawn around the tissue sections using a PAP pen. Sections were incubated with PBS-T for 15 minutes at room temperature. Sections were incubated with a permeabilization solution (PBS-T, 1% triton) for 30 minutes at room temperature. Sections were incubated with a blocking buffer solution (PBS-T, 1% BSA) for 30 minutes at room temperature or overnight at 4°C. Sections were washed three times for two minutes each with PBS-T. Sections were incubated with Trueblack Plus Lipofuscin Autofluorescence Quencher, 40X in DMSO (23014; Biotium) (40X solution was made into a working 1:40 dilution in PBS) for 5-10 minutes at room temperature. Sections were washed with PBS-T three times and then stained with a 1:200 dilution of primary antibodies, Anti-VZV (MAB8612; Sigma-Aldrich) and Anti-KRT15 (SAB4501658, Sigma-Aldrich), in a buffer solution (PBS-T, 1% BSA, 0.5% triton) for 1-2 hours at room temperature or overnight at 4°C. Sections were washed twice for two minutes with PBS-T then stained with a 1:1000 dilution of secondary antibodies, Goat anti-Mouse IgG AlexaFluor 568 (#A-11004; Invitrogen) and Donkey anti-Rabbit IgG AlexaFluor 488 (AB_2313584; Jackson ImmunoResearch), in a buffer solution (PBS-T, 1% BSA, 0.5% triton) for 60 minutes at room temperature in the dark. Sections were washed twice for two minutes with PBS-T. Coverslips were mounted using one drop of ProLong Diamond Antifade Mountant with DAPI (P36962; Thermo Fisher Scientific) and incubated at room temperature in the dark overnight. Microscopy was done on a Marianas system (3i) enclosed in an environmental chamber (Okolab) consisting of a Ziess Axio Observer 7 equipped with a X-Cite mini+ light source

(Excelitas) and a Prime BSI Express CMOS camera (Photometrics). Objectives used were 10X and 20X. Acquisition was done using SlideBook 6 (3i) and exported in Fiji for analysis and presentation.

	Antibody	Vendor	Host	Target	Dilution
Primary	Anti-VZV	Sigma-Aldrich	Mouse	VZV gE	1:200
	Anti-KRT15	Sigma-Aldrich	Rabbit	KRT15	1:200
Secondary	AlexaFluor 488	Jackson ImmunoResearch	Donkey	Rabbit	1:1000
	AlexaFluor 568	Invitrogen	Goat	Mouse	1:1000

Table 2. List of Antibodies

RESULTS

3.1 VZV-ORF57-Luc and mutants grew in cell culture in both HFF and ARPE-19 cells.

The viruses studied had mutations in the ORF62 region that is important for coding IE62, a protein necessary for viral replication. To determine if the mutations rendered any of the viruses defective for viral replication, VZV-OR57-Luc and the four mutants (62D_v1, 62D_v3, 68-62S-A, and 68-958) were grown from three different starting amounts (125 PFU/mL, 250 PFU/mL, and 500 PFU/mL) in HFF and ARPE-19 cells. We hypothesized that the mutations would stunt growth kinetics of the mutants in cells, at most, but viral replication. We chose a range of three starting amounts to better understand the not ablate growth kinetics of each virus. The growth rate could depend on the level of infection in the initial inoculum, so the differences in the growth rates were compared. Graphs of the raw total flux values (photons/second) obtained via IVIS^{TM} 50 imaging in both HFF (Fig. 1A-C) and ARPE-19 (Fig. 1D-F) cells are shown. Most of the mutants grew like the wild-type virus in both HFF and ARPE-19 cells. However, one mutant, 62D_v3, displayed stunted growth in HFF cells compared to the other viruses, especially at the 500 PFU inoculum (Fig. 1C). We concluded that the mutations did not ablate viral replication.

3.2 62D_v3, 68-62S-A and 68-958 had delayed and stunted growth in HFF cells compared to VZV-ORF57-Luc.

62D_v3 displayed a different growth phenotype than the VZV-ORF57-Luc and other mutant viruses in HFFs (Fig. 1C). Interestingly, 62D_v3 had a different phenotype than 62D_v1 – it's genomic twin. Both 62D_v1 and 62D_v3 have double mutations at S628G and R958G, differing only with the order the mutations were made; In 62D_v1,

R958G was made first, while in 62D_v3, S628G was made first. The growth delay in 62D_v3 warranted further investigation. We hypothesized that there was a difference in growth of 62D_v3 compared to 62D_v1 and VZV-ORF57-Luc in both cell types. Additionally, we hypothesized that the single mutants, 68-62S-A and 68-958, also had growth defects in both HFF and ARPE-19 cells.

The data from the first experiment was used for multiple analyses. To compare the viruses, we first chose an inoculation point that had roughly the same starting amount for the three wells. Scatterplots were made for DPI 0 (6-8 hours post-inoculation) and statistical analyses were done in both the HFF and ARPE-19 cells for each inoculation. We found that 500 PFU and 125 PFU in HFFs and ARPE-19s, respectively, were inoculated with roughly the same starting amount (Fig. 2A and D). To show the fold change of total flux for each virus, normalized values were calculated by normalizing each well to its DPI 0 value and then averaging between the three wells to generate the data point. A normalized graph of VZV-ORF57-Luc and double mutants, 62D_v1 and 62D_v3, at an inoculation of 500 PFU in HFF cells was created to show fold change of total flux (Fig. 2B). Scatterplots of the normalized values of each virus were created for each day and compared via an Ordinary one-way ANOVA Tukey's multiple comparisons test to determine statistical significance. The scatterplot for DPI 3 shows the relative trend for both VZV-ORF57-Luc and double mutants for each day (Fig. 2G). 62D_v3 grew more slowly and to a lower extent than VZV-ORF57-Luc and its genomic twin, 62D_v1, in HFFs. Interestingly, 62D_v1 had similar growth to VZV-ORF57-Luc in HFFs. This suggests there is a mutational defect in 62D_v3 that stunts growth in HFFs.

This process was repeated for VZV-ORF57-Luc and single mutants, 68-62S-A and 68-958 in HFFs at 500 PFU inoculation. The normalized graph of VZV-ORF57-Luc and single mutants demonstrated decreased growth of the single mutants as compared to VZV-ORF57-Luc (Fig. 2C). Scatterplots for each day were created and Ordinary one-way ANOVA Tukey's multiple comparisons test was used to determine statistical significance. DPI 3 was added to demonstrate the relative trend for VZV-ORF57-Luc and single mutants (Fig. 2H). Unlike the double mutants, both single mutants had slightly decreased growth compared to VZV-ORF57-Luc. Additionally, the single mutants grew at the same rate. The two single mutations may result in slightly defective but functional IE62 proteins.

These experiments were repeated in ARPE-19 cells but at an inoculation of 125 PFU because all viruses were at approximately the same starting amount at that concentration (Fig. 2D). There was no statistical significance between the fold changes of VZV-ORF57-Luc and the double mutants or VZV-ORF57-Luc and the single mutants (Fig. 2E and F). These results show that the mutants had no phenotype compared to VZV-ORF57-Luc in ARPE-19 cells. This could also suggest that in ARPE-19 cells, the mutational defect in 62D_v3 is either overcome or not present.

3.3 VZV-ORF57-Luc had decreased growth in ARPE-19 cells compared to HFF cells.

Wild-type VZV exhibits both slower and reduced growth in ARPE-19 cells compared to MRC-5 cells.[28] We set out to determine if VZV-ORF57-Luc would reproduce these findings. We hypothesized that VZV-ORF57-Luc would grow slower and to a lesser extent in ARPE-19 cells compared to HFF cells. Data from the growth kinetics experiment was used to address this question. To determine which inoculation

point to compare (125 PFU, 250 PFU, or 500 PFU), scatterplots of the DPIs 0 and 1 in both HFFs and ARPE-19s were compared (Fig. 3C and D) and analyzed. There was no statistical difference in inoculation at 250 PFU for both HFFs and ARPE-19s, so this data set was selected for analysis. VZV-ORF57-Luc growth in HFF and ARPE-19 cells was plotted using raw total flux values (p/s) measured via IVIS™ 50 imaging (Fig. 3A). A normalized graph of VZV-ORF57-Luc growth in both HFF and ARPE-19 cells was created to show fold change of total flux from each well normalized to the total flux at 6-8 hours post-inoculation (DPI 0) in the same well and then averaged between the three wells to generate the data point (Fig. 3B). VZV-ORF57-Luc did not grow as well in ARPE-19 cells on DPIs 4-7 (Fig. 3E-H and marked by asterisks in Fig. 3A and B). The results of the growth curve of VZV-ORF57-Luc in these two cell types showed that there is a phenotype of VZV-ORF57-Luc in ARPE-19 cells where VZV-ORF57-Luc growth is delayed at later times compared to HFF cells. The results were consistent with previous studies that demonstrated delayed growth of VZV in ARPE-19 cells compared to a fibroblast cell.[28] In this study, Graybill et al. also found that in ARPE-19 cells there was decreased expression and earlier decline of the transactivator protein, IE62, important for viral replication.[28]

3.4 62D_v3 displayed a severe growth defect in HFF cells compared to ARPE-19 cells.

From our previous experiments, we hypothesized that there was a severe growth defect in 62D_v3 in HFF cells but not in ARPE-19 cells but this phenotype would not be seen in the other mutants. The data from the growth kinetic experiment was analyzed to compare mutant virus growth in HFF and ARPE-19 cells. As before, we chose inoculation points that began with similar starting inoculations via statistical analyses in

each well on DPI 0 in HFF and ARPE-19 cells for each virus (data not shown). Normalized graphs of each mutant growth in HFF and ARPE-19 cells were created (Fig. 4A-D). As predicted, the three mutants, 62D_v1, 68-62S-A, and 68-958, grew similarly in HFF and ARPE-19 cells. 62D_v3 showed a marked decrease in rate and amount of viral growth in HFF cells compared to ARPE-19 cells on DPIs 2-7 (Fig. 4B, marked by asterisks). This confirmed that 62D_v3 was not only defective when compared to VZV-ORF57-Luc and other mutant viruses, it specifically had a growth defect in HFF cells.

3.5 vOka demonstrates similar growth in ARPE-19 cells compared to HFF cells.

HFF and ARPE-19 cells are both permissive for vOka. We hypothesized that vOka would have decreased growth in ARPE-19 compared to HFF cells, as reported in previous studies done by the Sadaoka group.[7] vOka was grown in HFF and ARPE-19 cells to determine if there was a phenotype in the different cell types. vOka growth in HFF and ARPE-19 cells was plotted using the values of the TCID50 assay (PFU/mL) (Fig. 5A). A normalized graph of vOka growth in HFF and ARPE-19 cells was created to show fold change with values from each well normalized to the calculated value of PFU/mL that was added in the initial inoculation (DPI 0), rather than a measured value, and these values were averaged (Fig. 5B). To determine if all the wells were inoculated with roughly the same starting amount, a scatterplot of the raw values from DPI 1 was compared (because there should not be a statistical significance in growth after one day if starting values were approximately the same). As expected, there were no significant differences between vOka growth in HFF and ARPE-19 cells on DPI 1 (Fig. 5C). A scatterplot of the raw values from DPIs 2-4 was made because the virus typically grows fastest then (Fig. 5D-F). Viral growth in HFF and ARPE-19 cells on DPIs 2 and 4 was

statistically different (marked by asterisks in Fig. 5A and B). However, the difference in vOka growth between ARPE-19 and HFF cells on certain days may not be biologically relevant because it was within a 1 log difference. We concluded that vOka grew similarly in HFF and ARPE-19 cells.

3.6 VZV-ORF57-Luc and mutants grew normally in the human skin explant model.

VZV is a human specific virus, making in vivo studies difficult without a proper animal model.[29] Development of a severe combined immunodeficiency (SCID-hu) mouse model allowed for human fetal thymus or skin xenografts implants, and this model has facilitated a better understanding of VZV and its mutant variants.[30] The necessity for studying VZV pathogenesis in human skin pushed development for alternative ex vivo methods, specifically skin organ culture (SOC). SOC was an ideal ex vivo model because while it not only contained both the epidermal and dermal layers it also had hair follicles and sebaceous glands. Additionally, SOC had the presence of all major cell types that were both positioned and differentiated, allowing VZV to be studied in a natural environment.[30] For these reasons, we chose the SOC model to move forward with our skin experiments.

We evaluated the mutants in skin to determine their phenotype, if any. From previous experiments, we hypothesized that three mutants would grow normally, but 62D_v3 would not. Breast tissue from reduction mammoplasty was inoculated with VZV-ORF57-Luc and four mutants in three different ranges of virus 100-400 PFU, 400-700 PFU, and 700-800 PFU to determine the growth kinetics in skin. This was done as a retrospective study on previous SOC experiments, so each inoculation curve represents a

different donor. We chose three different ranges of inoculum to determine if the starting amount affected growth patterns. Graphs of the raw total flux values (p/s) for VZV-ORF57-Luc and the four mutants in the skin are shown (Fig. 6A, C, E, G, I). Normalized graphs of VZV-ORF57-Luc and the four mutants in skin were created to show fold change of total flux from each skin piece normalized to the total flux value at DPI 1 and then averaged between the six values (Figures 6B, D, F, H, J). 450 PFU per skin piece was an ideal inoculation amount for mutant viruses that produced a growth curve most like the positive control, VZV-ORF57-Luc. VZV-ORF57-Luc typically decreases on DPI 3 and is followed by rapid growth on DPIs 4-14.[27] Our data matched this (Fig. 6A and B). Most mutants also displayed this phenotype in at least one inoculation point. Interestingly, a comparison of mutants across the same inoculation showed varied growth patterns. 62D_v3 grew at 360 PFU inoculation (Fig. 6E and F) and was like VZV-ORF57-Luc, while at the same inoculation, 68-958 (Fig. 6I and J) failed to grow at all. This may be due to either donor variability or a phenotype in the mutant viruses, but further investigation is warranted. We determined that all the mutant viruses were able to grow in skin.

3.7 Mutant viruses displayed no phenotypic difference in growth compared to VZV-ORF57-Luc, but there was variability in skin permissiveness for infection.

An interesting observation from the results of the growth kinetics experiment revealed variability in the growth patterns of mutants starting at the same inoculation point. To investigate further, we compared the mutant viruses and VZV-ORF57-Luc at a similar starting inoculum to determine if there were any differences between all the viruses' phenotypes in skin. We hypothesized that we would see differences in growth

kinetics of the mutant viruses between each other and with VZV-ORF57-Luc. Skin was inoculated with VZV-ORF57-Luc and four mutants. Data were combined from every SOC experiment where the average total flux ranged from 10^4 to10^6 p/s on DPI 1. This range was chosen because the IVIS™ 50 imaging background is approximately 10^4 p/s. This was done as a retrospective study on previous SOC experiments, so the data points are from different donors. To determine if the skin pieces were inoculated with the same starting amount, the total flux values from DPI 3 were analyzed and found to have no significant differences between the viruses (Fig. 7C). Graphs of the raw total flux values (p/s) (Fig. 7A) and the calculated normalized values (Fig. 7B) of the selected skin pieces are shown. To compare growth of the viruses, a scatterplot was made from the DPI 7 normalized values (Fig. 7D). DPI 7 was the chosen time point to analyze because the viral growth had stabilized after the initial decrease in growth on DPI 3 and subsequent increase on DPI 5. The viruses had similar growth on DPI 7. Interestingly, scatterplots of the raw and normalized values from each day showed a consistent divide between skin pieces that supported virus growth and pieces that did not. We used a 5-fold change of total flux as a cutoff for growth or no growth (Fig. 7D, dotted line) and calculated the percentage of infected skin pieces that supported 62D_v1, 62D_v3, 68-62S-A, 68-958, and VZV-ORF57-Luc growth as 21.21%, 35.1%, 45.24%, 28.57%, and 18.18%, respectively. We investigated if the variability in the growth was a phenotype of the viruses or if the true phenotype was masked by the skin pieces that did not support growth. The skin pieces that exceeded a 5-fold change on DPI 7 were analyzed separately to determine the viral phenotype, if any (Fig. 7E). Once again, we found no significant differences in viral growth of the mutants. We concluded that there was no significant

difference in viral growth of the mutants, but there was variability in skin permissiveness for viral growth.

3.8 VZV-ORF57-Luc induced abnormal KRT15 expression in skin.

There is evidence that vOka IE62 does not induce KRT15 expression in differentiated keratinocytes while pOka IE62 does (Cristina Tommasi, unpublished results). It was not known if VZV-ORF57-Luc, which is derived from pOka, would induce KRT15 expression in skin. The SOC model uses differentiated adult skin, which expresses KRT15 constitutively in the basal layer of the epidermis and the bulge area of hair follicles.[19] We hypothesized that VZV-ORF57-Luc would induce abnormal expression of KRT15. To evaluate the effects of wild-type VZV infection on KRT15 expression in skin, we used immunofluorescence microscopy on paraffin-embedded and sectioned tissues. The skin was inoculated with VZV-ORF57-Luc infected HFFs then prepared for antibody detection of KRT15 and VZV gE. All slides were prepared and stained on the same day and images were collected at the same exposure settings. Negative controls from DPI 1 and DPI 14 were slides treated with the secondary antibodies only. The images collected for the negative controls were used to subtract background signals on both DPI 1 and DPI 14 slides that were treated with both primary and secondary antibodies. Baseline signals, representing constitutive KRT15 expression, were measured from the DPI 1 slide stained with both primary and secondary antibodies (Fig. 8A). At DPI 1, infection was widely scattered (not visible in this image) and the epidermis was intact (Fig. 8A, KRT15 panel). Additionally, this slide was used to ascertain that dermarolling did not cause wounds that induced KRT15 expression (Fig. 8A, KRT15 panel). DPI 1 skin was a good “uninfected” control because it provides a

landscape of how an inoculated piece of skin appears before infection spreads. Using the DPI 1 skin, we subtracted baseline signals from DPI 14 skin to determine the background threshold.

As expected, KRT15 was expressed along the basal layer and scattered throughout the epidermis (Fig. 8B-E). VZV gE was detected in widely dispersed regions in the epidermis and the dermis. There was an overlap of KRT15 and gE in tracks in the dermis and vesicular lesions in the epidermis. Notably, panels C and D are images of serial sections of the same skin piece on two separate slides. The KRT15 and gE colocalization was consistent, demonstrating that the antibody detection was reliable and not from an artifact. Specifically, from panels C and D, a magnified image (Fig. 8G and H, white arrows) of a blood vessel track in the dermis had gE expression and KRT15 activation in a site where KRT15 is not normally observed. These results show that after 14 days, VZV spread through the epidermis, causing cell death, as DAPI staining was absent in these layers, whilst activating KRT15 expression. Panels B and E are further examples of gE overlap with KRT15 activation and expression, particularly in the dermal layers and outer epidermal layers of tissue. Panel B was magnified to show the colocalization of gE and KRT15 in the dermis (Fig. 8F). These results demonstrate that VZV-ORF57-Luc infection activated KRT15 expression in infected cells.

3.9 Single mutant virus, 68-62S-A, induced abnormal KRT15 expression in skin.

The mutant viruses had changes in ORF62 that could affect IE62 functions. Hence, the mutations might also affect KRT15 expression. We hypothesized that 68-62S-A would induce KRT15 expression, but we did not know to what extent. To evaluate the effects of the vaccine SNP, S628G, on KRT15 expression in the skin, we performed

immunofluorescence microscopy. The experiment was performed on the same day as VZV-ORF57-Luc and images were taken on the same day so that the results could be compared. Figure 9A panels represent the DPI 1 uninfected control. KRT15 expression displayed the normal pattern and VZV gE was sparse (Fig. 9B and C). Where gE was detected, in a VZV-induced lesion where the basal and outer epidermal layers of skin had separated (Fig. 9B), there was no overlap with KRT15. Additionally, a characteristic multinucleated cell was observed (Fig. 9C and D, DAPI panel, white arrow). However, this typical sign of VZV infection was not associated with KRT15 upregulation. These results showed that 68-62S-A had similar characteristics to normal VZV infection but did not induce KRT15 to the same extent as wild-type VZV-ORF57-Luc.

3.10 Single mutant virus, 68-958, induced abnormal KRT15 expression in skin.

Like 68-62S-A, 68-958 also has a single mutation in the ORF62 region that may affect IE62 expression and, therefore, KRT15 expression. To evaluate the effects of the vaccine SNP, R958G, on KRT15 expression in the skin, we performed immunofluorescence microscopy. The experiments and images were performed and collected by the same method as both VZV-ORF57-Luc and 68-62S-A. Figure 10A panels represent the DPI 1 uninfected control. The mutant strain 69-958 grew well in skin and VZV gE was detected widely in epidermal lesions (Fig. 10B and E), in hair follicles (Fig. 10C and F), and tracks in the dermis (Fig.10D and G). KRT15 was induced in cells expressing gE in keratinocytes in the dermis and hair follicle, but not in the dermal track or other dermal cells. Interestingly, where virus infection penetrated the dermal layer (Fig. 10B and E, Merge panel, white arrows and bracket), KRT15 expression did not overlap, suggesting that this mutation may affect KRT15 expression in dermal cells. The

identity of these dermal cells is not known, although dermal fibroblasts, myeloid cells, T lymphocytes, and endothelial cells are abundant in the dermis. These results show that VZV strain 68-958 grew in the skin and induced KRT15 expression in keratinocytes but not in dermal cells.

DISCUSSION

The biological mechanism of vOka attenuation in skin has long been difficult to elucidate due to its genetic heterogeneity. Through whole genome sequencing, we know that 137 core SNPs are consistent, with six being near fixed and stable across all vOka preparations.[6] These six SNPs are found in ORF62, a gene that encodes a VZV transcriptional regulatory protein, IE62, important for VZV replication and an early indicator of VZV infection.[14,23] Another protein found to be abnormally upregulated with VZV infection is KRT15, although the expression is not solely confined to VZV-infected cells and the mechanism for upregulation is not well understood.[23] We hypothesized that SNPs in ORF62 are responsible for vOka attenuation in skin through IE62 regulation of KRT15 expression.

To test our hypothesis, Dr. Kinchington created four mutant viruses based on SNPs with fixed or nearly fixed (98-100%) average allele frequencies found across four licensed Oka vaccine strains.[6] The mutant viruses had amino acid changes at two sites of interest, 628 and 958. The SNP in 628 changes the amino acid from a polar serine in pOka to a nonpolar glycine. The SNP in 958 changes the amino acid from a polar, charged arginine in pOka to a nonpolar glycine. Two mutant viruses, 62D_v1 and 62D_v3, had mutations in both 628 and 958 that were made in different orders, with R958G made first in v1 and S628G made first in v3. The other mutant viruses, 68-62S-A and 68-958, have single mutations in nucleotides 628 and 958, respectively.

The mutant viruses 62D_v3, 68-62S-A, and 68-958 had a delayed growth phenotype in HFFs compared to VZV-ORF57-Luc, the wild-type recombinant virus. This was not seen in ARPE-19 cells. VZV successfully infects quiescent cells, including the contact-inhibited HFFs, and induces replication via activation of cyclin-dependent

kinases.[31] These viruses have mutations in ORF62, a transcription factor that is important for VZV replication, which may be one reason for the growth delay in HFFs compared to the WT virus. Specifically, the 62D_v3 strain displayed a delayed growth phenotype not only in HFFs compared to the WT virus but also compared to its growth in ARPE-19s. This same phenotype was not seen in its counterpart, 62D_v1. Both 62D mutants should have identical genome profiles, yet 62D_v1 displayed similar growth kinetics to VZV-ORF57-Luc in HFFs and ARPE-19s while 62D_v3 did not. Possible explanations for this phenomenon include extraneous mutations during the virus isolation process, loss of virulence during passage in cell culture, or an unknown phenomenon that occurs when nucleotides are mutated in a particular order. In addition, previous studies have found that VZV infection in ARPE-19 cells leads to decreased levels and earlier decline of IE62 expression.[28] 62D_v3 growth in ARPE-19 cells was not different than VZV-ORF57-Luc or the other viral mutants, suggesting that the IE62 expression that is normally expressed in ARPE-19 cells is not changed. Instead, the defect in 62D_v3 may be related to the HFF-specific cyclin dependent kinases. To explore this further, the double mutant viruses should be sequenced to confirm their genetic profiles. In addition, it would be interesting to quantify IE62 expression of 62D_v3 in both cell types. These experiments showed that the SNPs in the mutant viruses affected growth in cells. Unfortunately, the mutants could not be directly compared to vOka using bioluminescence imaging because vOka does not express luciferase and must be measured via TCID50 assays. Future studies should focus on evaluating growth kinetics in cells using one method to compare all the viruses.

Except for 62D_v3, all the mutant viruses, VZV-ORF57-Luc, and vOka demonstrated increased growth in HFFs compared to ARPE-19s. VZV-ORF57-Luc

growth in both cell types diverged on days 4-7, where there was a decreased growth rate in ARPE-19 cells. This is consistent with previous literature showing decreased growth of cell-associated VZV in ARPE-19 cells starting on day 4 and onwards.[28] For vOka, there was also a significant delay in growth on days 2 and 4 in ARPE-19 cells. One possible explanation could have been that the difference was attributed to both viruses being propagated in HFFs and remaining cell-associated for these experiments. While plausible, this theory is unlikely due to WT and vOka viruses being harvested at a very high infectivity rate so there are few uninfected HFFs that would be plated with infected HFFs. Another, more plausible, theory is that there is a decrease in VZV IE62 expression from ORF62, an important transcription factor for inducing cell division and replication, in ARPE-19 cells. As mentioned previously, IE62 expression in VZV-infected ARPE-19 cells was markedly decreased after day 3 of infection.[28] While both VZV-ORF57-Luc and vOka demonstrated a decreased growth rate in ARPE-19 cells compared to HFFs, all the viral mutants showed either an increase or a nonsignificant difference from HFFs that may be due to the differences in IE62 expression from the mutations in the ORF62 region. To explore further, western blots for IE62 expression from all viruses should be performed.

While the mutant viruses were different from wild type VZV in cells, we were surprised to find no significant differences in viral growth in skin. One interesting observation was a consistent divide between skin pieces that supported virus growth and pieces that did not. Unfortunately, we did not have vOka measurements as it is not luciferase expressing and could not be measured using the IVIS™ 50. These results suggest that viral entry and/or infection was not successful in the skin explants. This

could be due to many reasons including human inconsistencies, the inoculation protocol, or decreased viral virulence. Another plausible explanation for why certain skin was permissive to growth would be the status of donor immunity. For VZV to establish infection, it must overcome innate antiviral upregulation of cellular cytokines. If a donor has a particularly healthy immune system, VZV might not overcome the immune response. This point is especially relevant because the skin is donated anonymously from patients undergoing elective reduction mammoplasty. In a retrospective analysis looking at 20,000 women who underwent elective reduction mammoplasty from 1965 to 1993, 63% of patients were under the age of 40.[32] Barring any genetic diseases, this age group can be assumed to have a healthy immune system. If we assume similar demographics of the people who donated skin for this study, it is likely they have robust innate immune defenses that the viruses must overcome to establish infection.

In the skin pieces where VZV established infection, KRT15 expression was induced, as predicted, especially in conjunction with VZV-ORF57-Luc and 68-958 infection. In skin, KRT15 expression is normally found in areas with stem cells, particularly the basal layer of the epidermis and the bulge area of hair follicles.[21] In previous studies using epidermal keratinocytes, VZV upregulated KRT15 preferentially in undifferentiated keratinocytes predominantly in the basal layer of the epidermis.[23] Our immunofluorescence microscopy results in skin were consistent with the findings in keratinocytes, and we also detected KRT15 expression associated with VZV infection not only in the bulge area of hair follicles but also the dermis, far from the stem cells of the basal layer or hair follicles. This suggests that VZV infection can activate KRT15, a putative stem cell marker, at a distance from stem cells. Another interesting observation

was that unlike VZV-ORF57-Luc and 68-958, 68-62S-A had no overlapping VZV and KRT15 expression. Instead, around the areas of VZV infection, KRT15 expression appeared either downregulated or turned off. This could suggest that IE62 with the SNP in nucleotide 628 does not activate KRT15. Additionally, the KRT15 expression pattern in 68-958 must be explored further, particularly due to the importance of the 100% conserved nature of this SNP. The absence of KRT15 induction in the dermis compared to the upregulation seen in VZV-ORF57-Luc may be the reason for attenuation. In preliminary studies, VZV infection was stunted with the absence of KRT15 expression and, further, vOka did not express KRT15, strengthening the correlation of the relationship between KRT15 expression and attenuation. The lack of KRT15 may prevent upregulation of the DDR that helps cells repair damaged DNA instead of undergoing apoptosis. The DDR is activated as a cellular response to viral infection, but it can ultimately help and enhance virus replication.[25] Cells with DNA damage will induce kinases that phosphorylate DDR proteins like H2AX, a histone protein that helps to repair DNA.[25] VZV infection has found to induce the phosphorylation of H2AX.[25] Many lymphocytes, like T cells, NK cells, and B cells, are found in the dermis of the skin[33] and may be able to combat the infection, especially in the absence of KRT15 expression.

Future studies should address the status of KRT15 expression in skin infected with vOka, 62D_v1, and 62D_v3 by immunofluorescence microscopy. In addition, quantifying KRT15 and VZV proteins via western blots could reveal a correlation between the levels of infection needed to activate KRT15. It would also be interesting to quantify cytokine or inflammatory markers with KRT15 expression and VZV infection to evaluate the innate immune responses. There are still many gaps in our understanding of

the mechanism of vOka attenuation in skin. The results of our studies have shown promising data that may elucidate the relationship between the conserved vaccine SNPs, KRT15 expression, and levels of VZV infection.

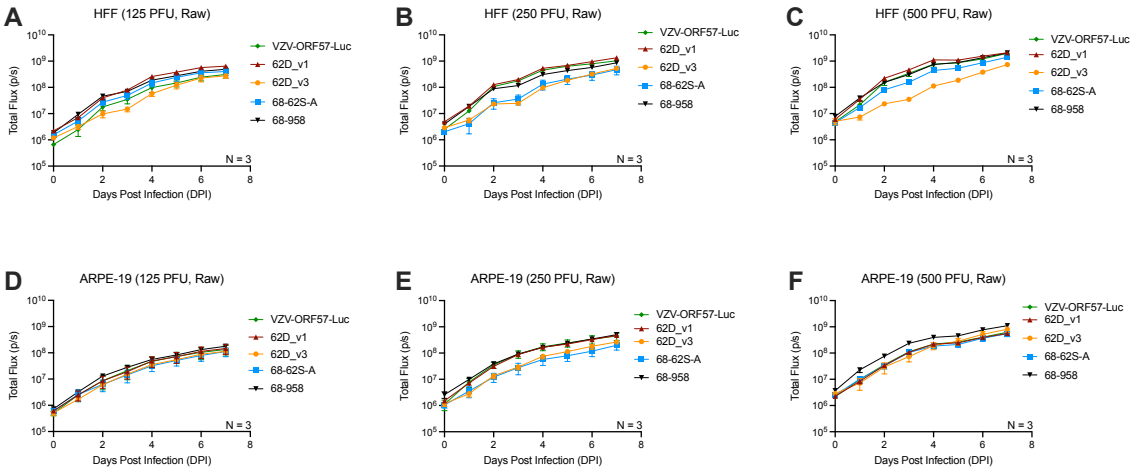

Figure 1 VZV-ORF57-Luc and mutants grew in cell culture in both HFF and ARPE-19 cells. HFF and ARPE-19 cell monolayers were inoculated with VZV-ORF57-Luc or mutant viruses 62D_v1, 62D_v3, 68-62S-A, and 68-958 at three concentrations: 125 PFU, 250 PFU, or 500 PFU. Virus spread was measured by bioluminescence via IVIS™ 50 imaging. Each point is the average of triplicate wells (N=3), and the error bar indicates standard deviation. All viruses grew in both cell types. Raw total flux (photons/second) values in HFF cells at: (A), 125 PFU inoculation (B), 250 PFU inoculation, and (C), 500 PFU inoculation. Raw total flux (p/s) values in ARPE-19 cells at: (D), 125 PFU inoculation (B), 250 PFU inoculation, and (C), 500 PFU inoculation.

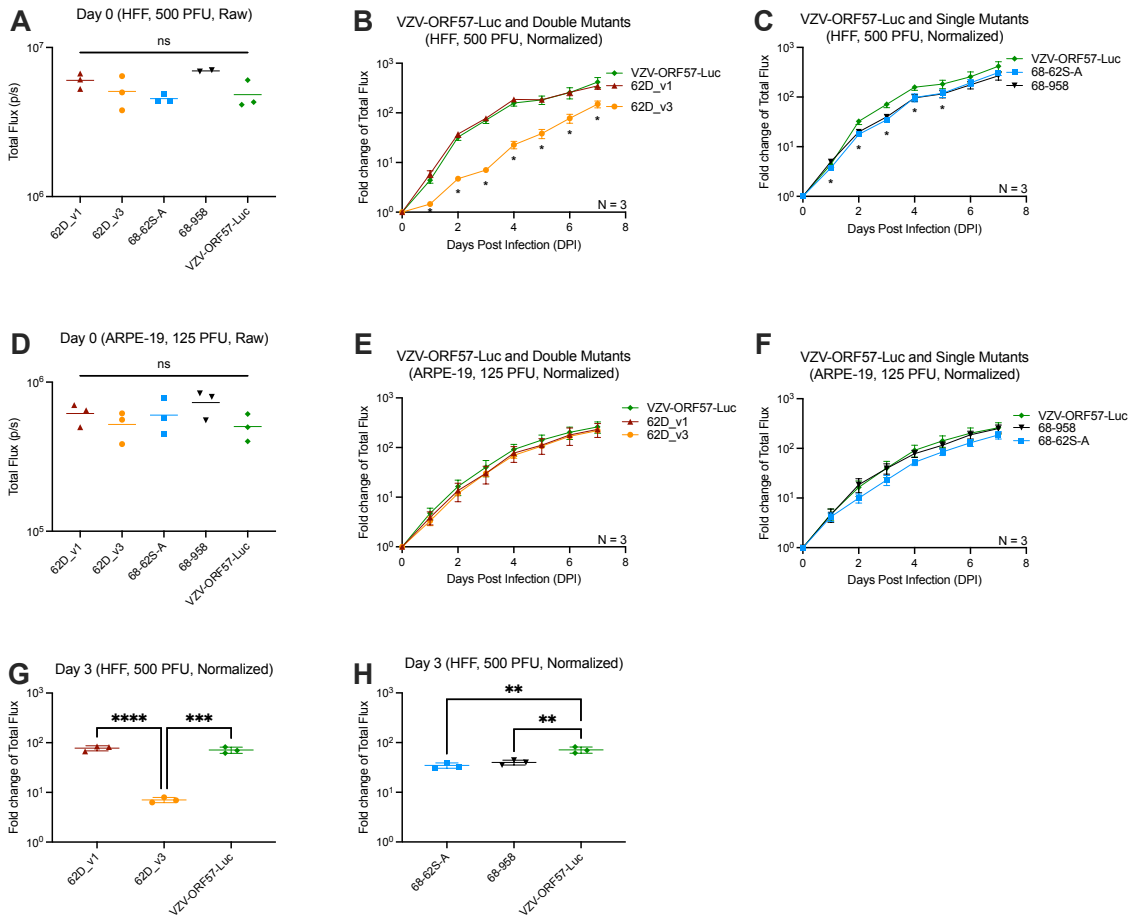

Figure 2 62D_v3, 68-62S-A and 68-958 had delayed and stunted growth in HFF cells compared to VZV-ORF57-Luc. HFF and ARPE-19 cell monolayers with 500 and 125 PFU inoculations, respectively, of VZV-ORF57-Luc or mutant viruses, 62D_v1, 62D_v3, 68-62S-A, and 68-985. Virus spread was measured by bioluminescence via IVIS™ 50 imaging. Each point is the average of triplicate wells (N=3), and the error bar indicates standard deviation. On DPIs 0 and 3, the individual measurements are shown for statistical analyses with a bar at the mean. Values were compared via Ordinary one-way ANOVA Tukey's multiple comparisons test, * indicates $p \leq 0.05$ and ns indicates not significant. (A), Raw total flux (photons/second) values of all viruses on DPI 0 in HFF cells at 500 PFU inoculation (B), Normalized graph of VZV-ORF57-Luc, 62D_v1, and 62D_v3 in HFF cells at 500 PFU inoculation (C), Normalized graph of VZV-ORF57-Luc, 68-62S-A, and 68-958 in HFF cells at 500 PFU inoculation (D), Raw total flux (p/s) values of all viruses on DPI 0 in ARPE-19 cells at 125 PFU inoculation (E), Normalized graph of VZV-ORF57-Luc, 62D_v1, and 62D_v3 in ARPE-19 cells at 125 PFU inoculation (F), Normalized graph of VZV-ORF57-Luc, 68-62S-A, and 68-958 in ARPE-19 cells at 125 PFU inoculation (G), Scatterplot of DPI 3 normalized values of VZV-ORF57-Luc, 62D_v1, and 62D_v3 in HFF cells at 500 PFU inoculation (H), Scatterplot of DPI 3 normalized values of VZV-ORF57-Luc, 68-62S-A, and 68-958 in HFF cells at 500 PFU inoculation.

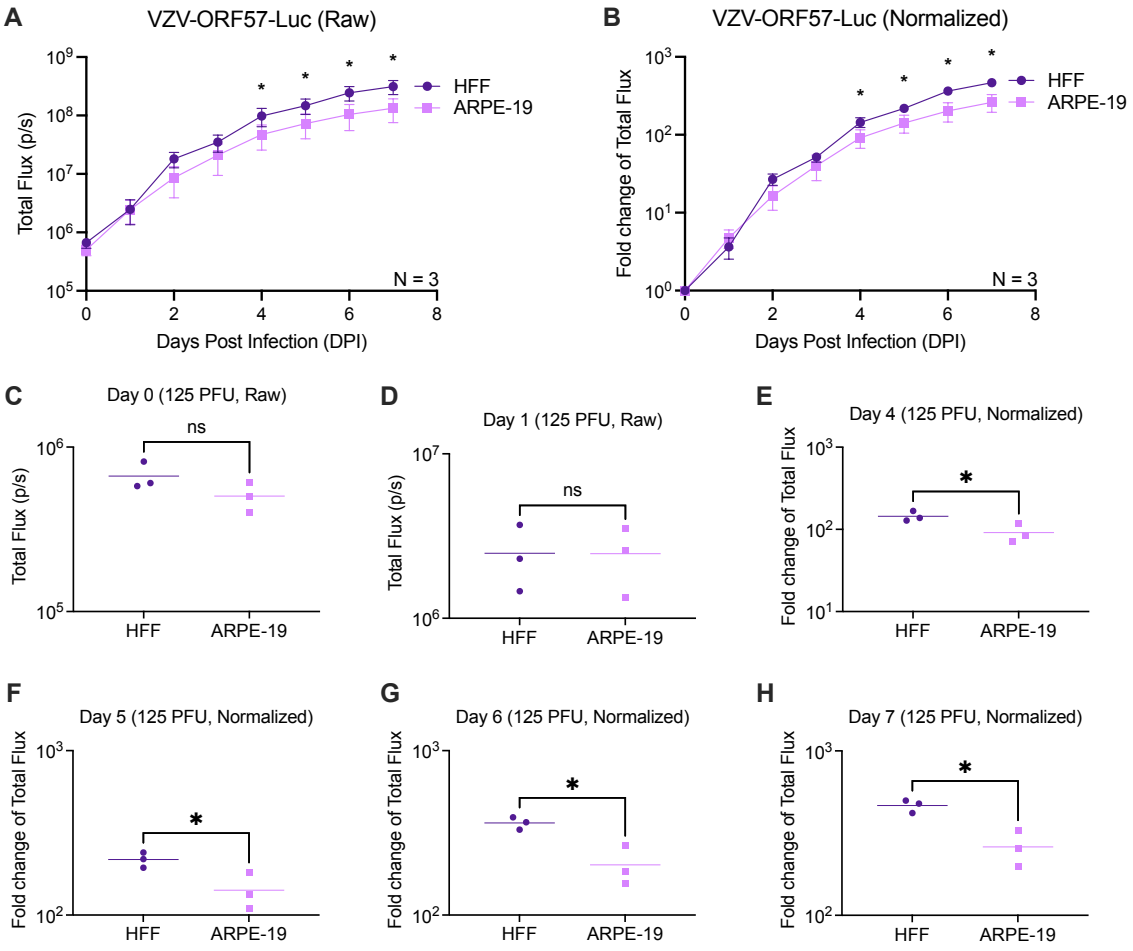

Figure 3 VZV-ORF57-Luc had decreased growth in ARPE-19 cells compared to HFF cells. HFF and ARPE-19 cell monolayers were inoculated with 125 PFU VZV-ORF57-Luc. Virus spread was measured by bioluminescence via IVIS™ 50 imaging. Each point is the average of triplicate wells (N=3), and the error bar indicates standard deviation. On DPIs 0, 1, and 4-7, the individual measurements are shown for statistical analyses with a bar at the mean. Values were compared via unpaired Student's t-test, * indicates $p \leq 0.05$ and ns indicates not significant. (A), Growth curve of raw total flux (photons/second) values of VZV-ORF57-Luc in HFF and ARPE-19 cells with 125 PFU inoculation (B), Normalized growth curve of VZV-ORF57-Luc in HFF and ARPE-19 cells with 125 PFU inoculation (C and D), Raw total flux (p/s) values of VZV-ORF57-Luc on DPIs 0 and 1 in HFF and ARPE-19 cells at 125 PFU inoculation (E-H), Normalized values of VZV-ORF57-Luc on DPIs 4-7 in HFF an ARPE-19 cells at 125 PFU inoculation.

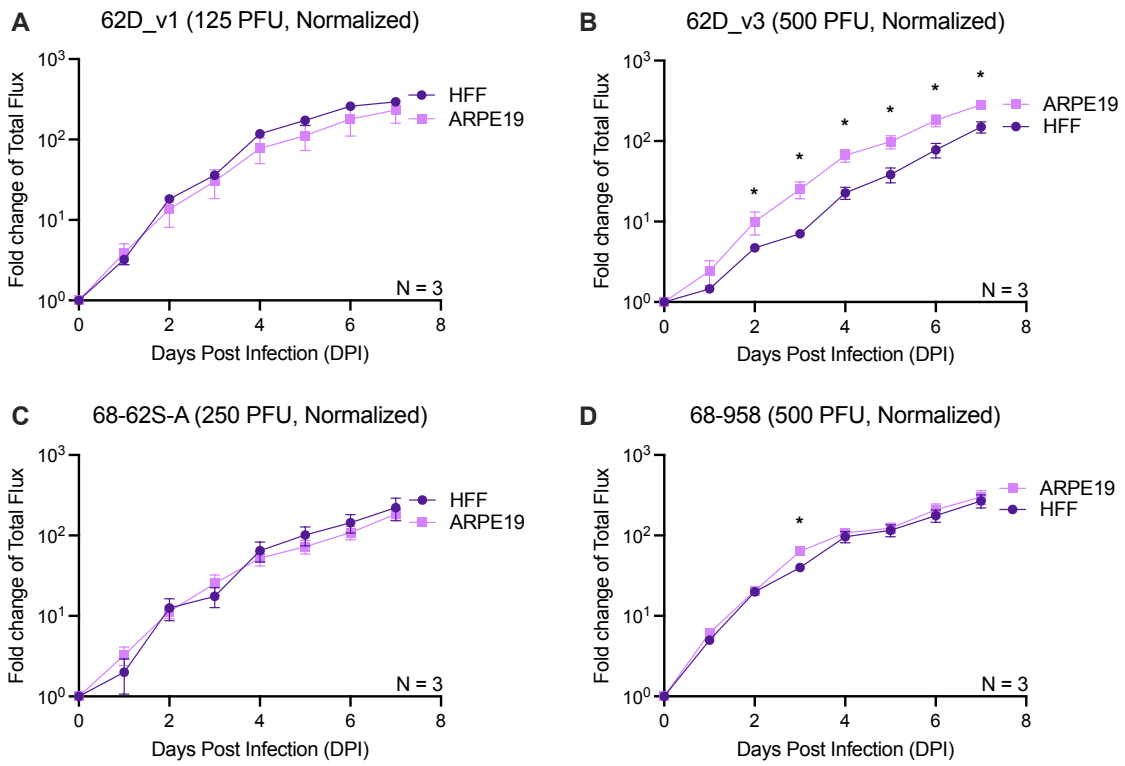

Figure 4 62D_v3 displayed a severe growth defect in HFF cells compared to ARPE-19 cells. HFF and ARPE-19 cell monolayers were inoculated with 125, 250 or 500 PFU of mutant viruses, 62D_v1, 62D_v3, 68-62S-A, or 68-958. Virus spread was measured by bioluminescence via IVIS™ 50 imaging. Each point is the average of triplicate wells (N = 3), and the error bar indicates standard deviation. Values were compared via unpaired Student's t-test, * indicates $p \leq 0.05$. (A), Normalized graph of double mutant virus, 62D_v1, in both HFF and ARPE-19 cells at 125 PFU inoculation (B), Normalized graph of double mutant virus, 62D_v3, in both HFF and ARPE-19 cells at 500 PFU inoculation (C), Normalized graph of single mutant virus, 68-62S-A, in both HFF and ARPE-19 cells at 250 PFU inoculation (D), Normalized graph of single mutant virus, 68-958, in both HFF and ARPE-19 cells at 500 PFU inoculation.

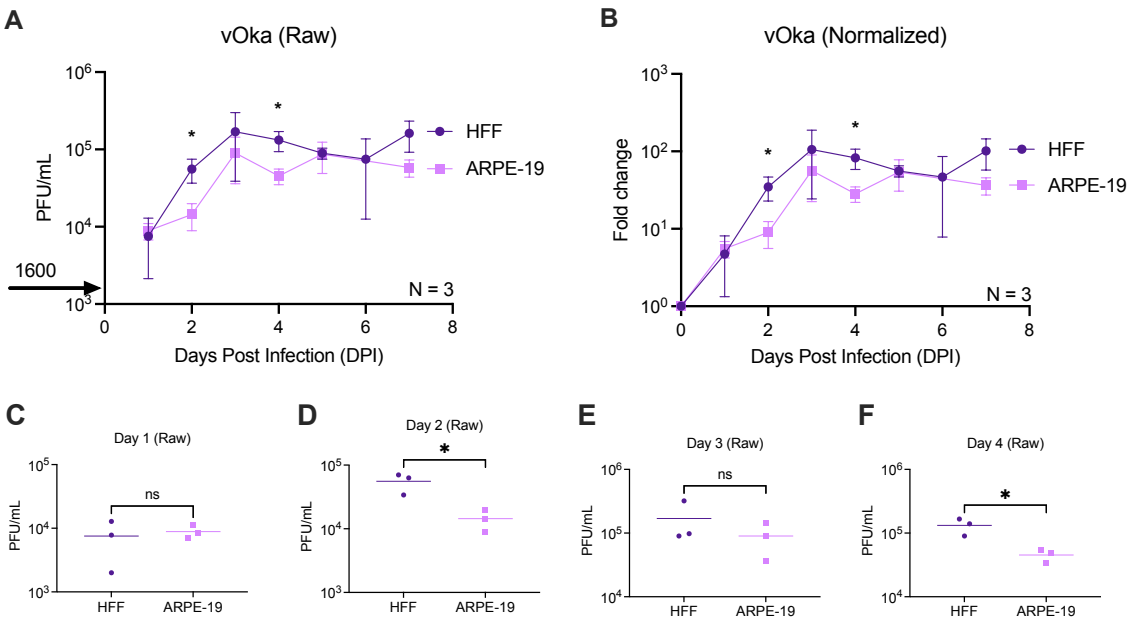

Figure 5 vOka demonstrates similar growth in ARPE-19 cells compared to HFF cells. HFF and ARPE-19 cell monolayers were inoculated with 1600 PFU of vOka. Virus spread was measured by TCID50 assay. Each point is the average of triplicate wells (N = 3), and the error bar indicates standard deviation. On DPIs 1-4, the individual measurements are shown for statistical analyses with a bar at the mean. Values were compared via unpaired Student's t-test, * indicates $p \leq 0.05$ and ns indicates not significant. (A), Growth curve of vOka in HFF and ARPE-19 cells with 1600 PFU inoculation using TCID50 assay (B), Normalized growth curve of vOka in HFF and ARPE-19 cells with 1600 PFU inoculation (C-F), TCID50 assay calculated values of vOka on DPIs 1-4 in HFF and ARPE-19 cells.

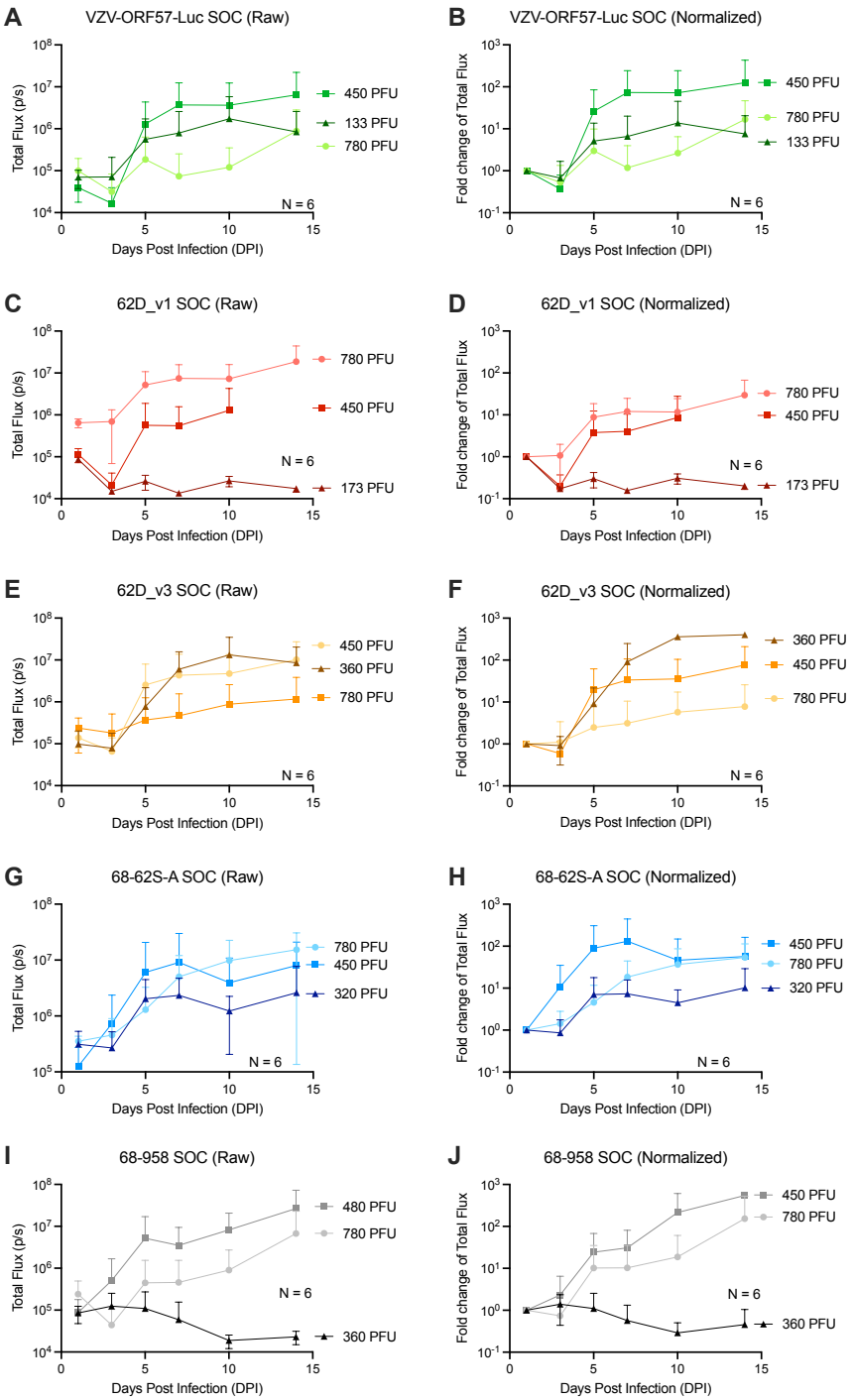

Figure 6 VZV-ORF57-Luc and mutants grew normally in the human skin explant model. Skin pieces were inoculated with three concentration ranges 100-400 PFU, 400-700 PFU, or 700-800 PFU of VZV-ORF57-Luc or mutant viruses 62D_v1, 62D_v3, 68-62S-A, and 68-958. Virus spread was measured by bioluminescence via IVIS™ 50 imaging. Each point is the average of six (N=6) skin pieces, and the error bar indicates standard deviation. Raw total flux values (photons/second) and normalized values were graphed for: (A, B), VZV-ORF57-Luc (C, D), 62D_v1 (E, F), 62D_v3 (G, H), 68-62S-A (I, J), 68-958.

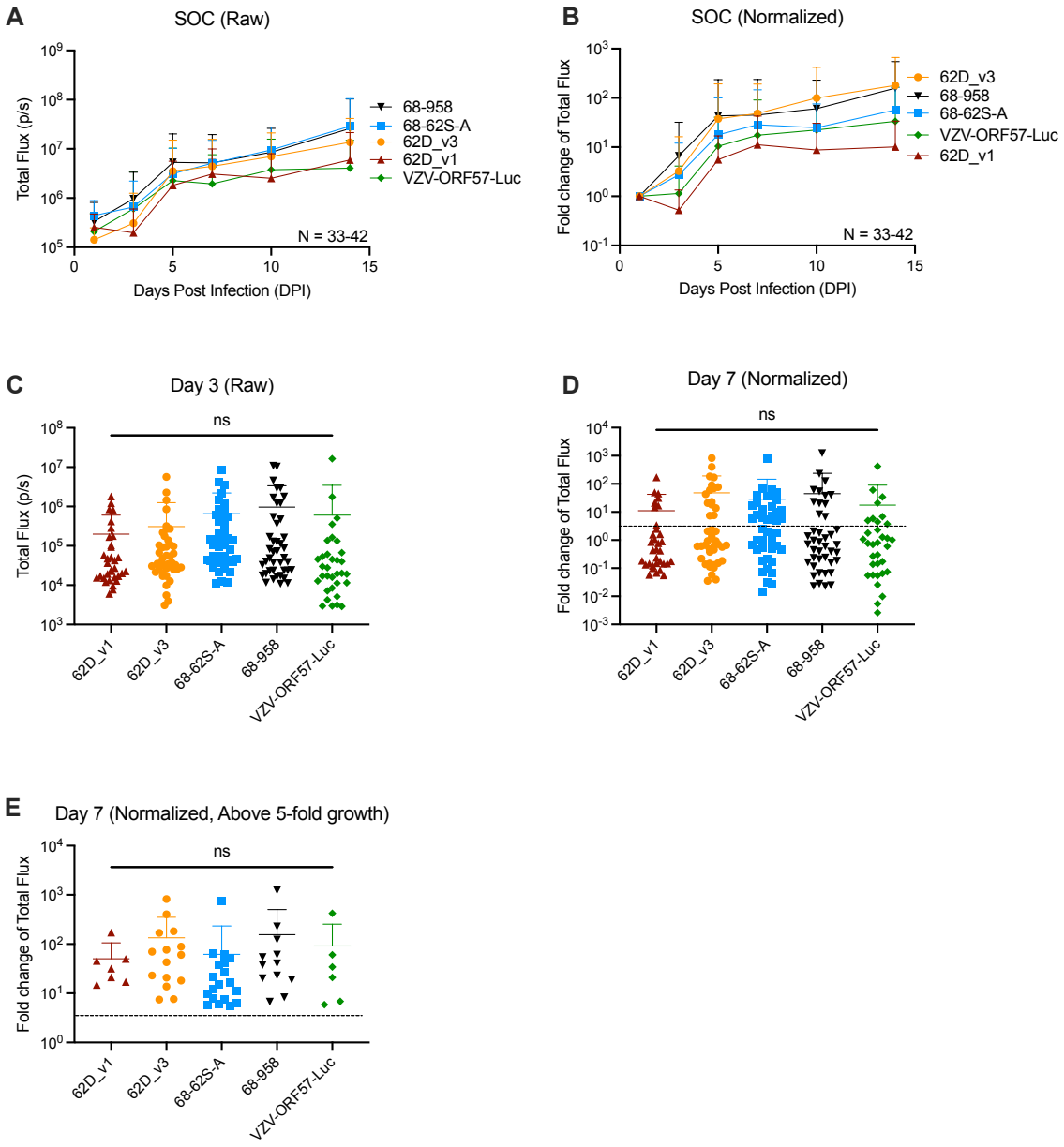

Figure 7 Mutant viruses displayed no phenotypic difference in growth compared to VZV-ORF57-Luc, but there was variability in skin permissiveness for infection. Skin pieces were inoculated with VZV-ORF57-Luc or mutant viruses 62D_v1, 62D_v3, 68-62S-A, and 68-958. Virus spread was measured by bioluminescence via IVIS™ 50 imaging. The error bar indicates standard deviation. On DPIs 3 and 7, the individual measurements are shown for statistical analyses with a bar at the mean. Values were compared via Ordinary one-way ANOVA Tukey's multiple comparisons test, * indicates $p \leq 0.05$ and ns indicates not significant. (A), Growth curve of raw total flux values (photons/second) of all viruses (B), Normalized growth curve of all viruses (C), Scatterplot of DPI 3 raw total flux values (p/s) (D), Scatterplot of DPI 7 normalized values. Dotted line marks 5-fold change (E), Scatterplot of DPI 7 normalized values that were above a 5-fold growth change.

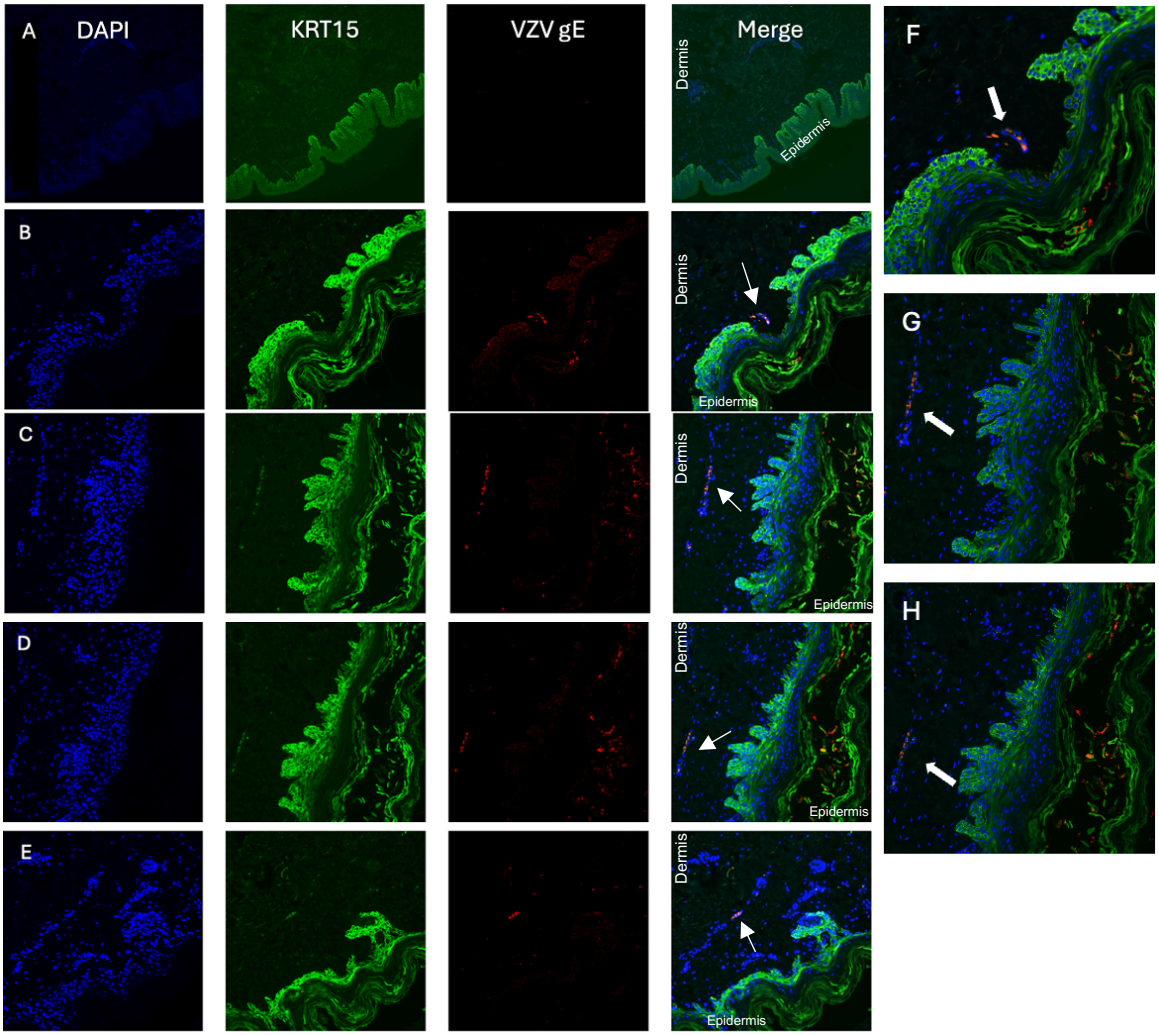

Figure 8 VZV-ORF57-Luc induced abnormal KRT15 expression in skin. Skin was inoculated with VZV-ORF57-Luc infected HFFs and collected after DPIs 1 and 14. Original magnification (x10) on a Marianas Microscope; DAPI – 4;6-diamidino-2-phenylindole; KRT15 – Cytokeratin 15; VZV gE – Varicella Zoster Virus Glycoprotein I. (A), DPI 1 uninfected skin (B), DPI 14 infected skin with KRT15 and VZV expression in dermis (C), DPI 14 infected skin with epidermal lesion and blood vessel tract in dermis (D), DPI 14 infected skin with epidermal lesion and blood vessel tract in dermis (E), DPI 14 infected skin with blood vessel tract in dermis (F), Magnified image from Merge of Panel B; white arrow to blood vessel (G), Magnified image from Merge of Panel C; white arrow to blood vessel (H), Magnified image from Merge of Panel D; white arrow to blood vessel.

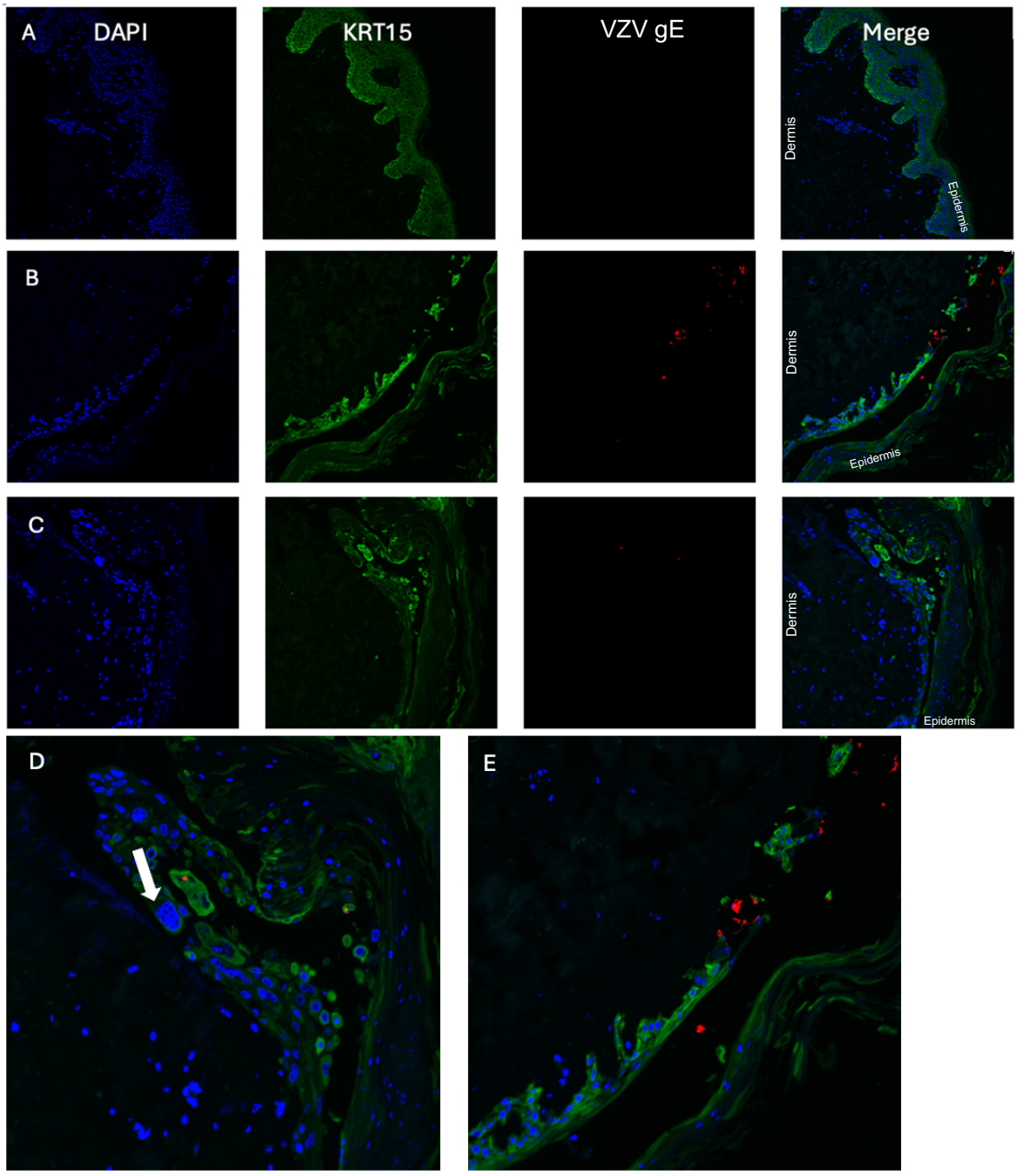

Figure 9 Single mutant virus, 68-62S-A, induced abnormal KRT15 expression in skin. Skin was inoculated with 68-62S-A infected HFFs and collected after DPIs 1 and 14. Original magnification (x10 and x20) on a Marianas Microscope; DAPI – 4;6-diamidino-2-phenylindole; KRT15 – Cytokeratin 15; VZV gE – Varicella Zoster Virus Glycoprotein I. (A), DPI 1 uninfected skin (B), DPI 14 infected skin with KRT15 and VZV expression in epidermis (C), DPI 14 infected skin with multinucleated cell (D), Magnified image from Merge of Panel C; white arrow to multinucleated cell (E), Magnified image from Merge of Panel B.

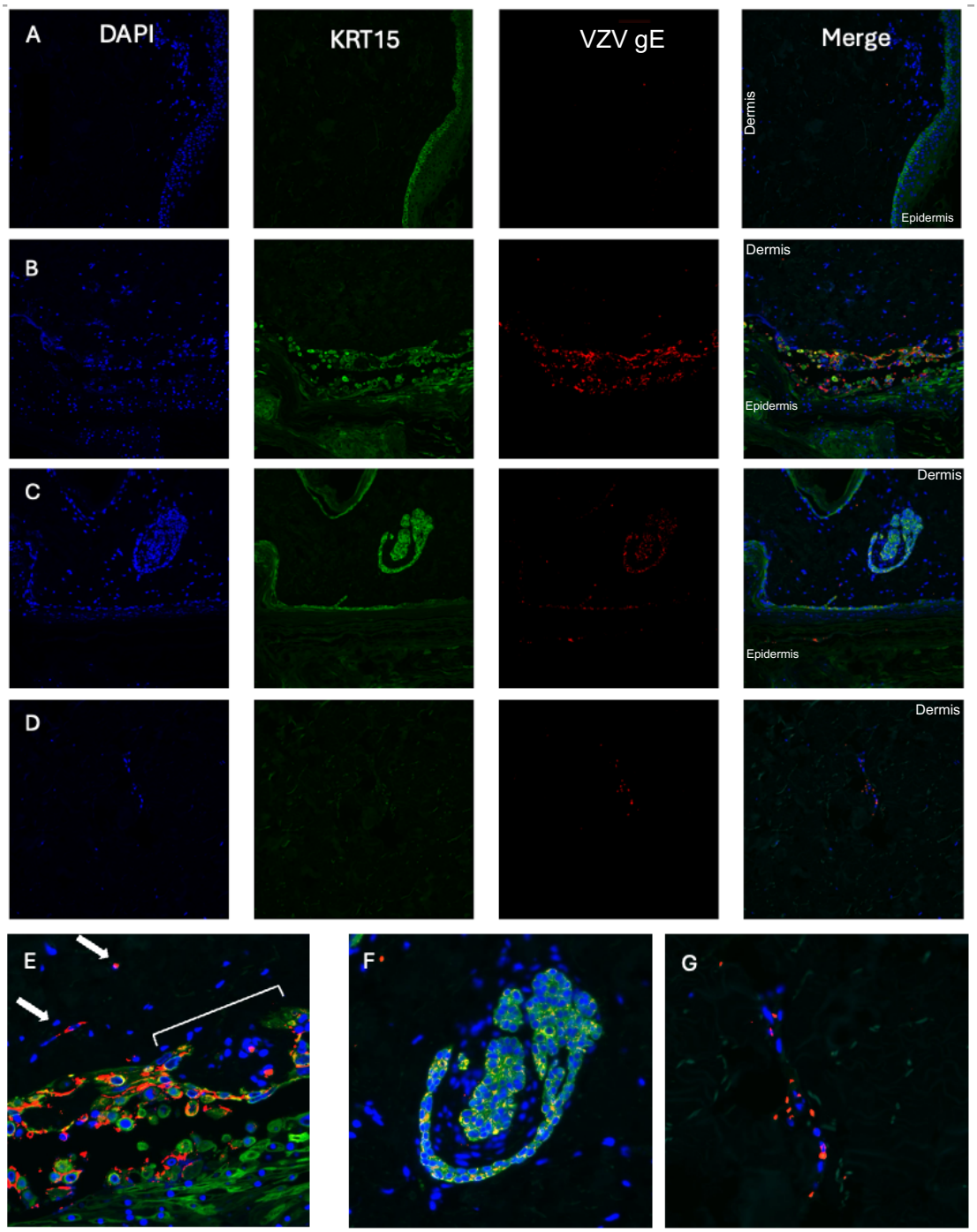

Figure 10 Single mutant virus, 68-958, induced abnormal KRT15 expression in skin. Skin was inoculated with 68-958 infected HFFs and collected after DPIs 1 and 14. Original magnification (x10 and x20) on a Marianas Microscope; DAPI – 4;6-diamidino-2-phenylindole; KRT15 – Cytokeratin 15; VZV gE – Varicella Zoster Virus Glycoprotein I. (A), DPI 1 uninfected skin (B), DPI 14 infected skin with KRT15 and VZV expression in epidermis (C), DPI 14 infected skin with hair follicle (D), DPI 14 infected skin with blood vessel tract in dermis (E), Magnified image from Merge of Panel B; white arrow to blood vessel and white bracket to epidermal lesion (F), Magnified image from Merge of Panel C of hair follicle (G), Magnified image from Merge of Panel D; blood vessel.

REFERENCES

1. Arvin AM. Creating the “Dew Drop on a Rose Petal”: the Molecular Pathogenesis of Varicella-Zoster Virus Skin Lesions. *Microbiol Mol Biol Rev MMBR*. 2023;87(3):e0011622. doi:10.1128/mmbr.00116-22

2. Lei V, Petty AJ, Atwater AR, Wolfe SA, MacLeod AS. Skin Viral Infections: Host Antiviral Innate Immunity and Viral Immune Evasion. *Front Immunol*. 2020;11. doi:10.3389/fimmu.2020.593901

3. Zerboni L, Sen N, Oliver SL, Arvin AM. Molecular mechanisms of varicella zoster virus pathogenesis. *Nat Rev Microbiol*. 2014;12(3):197-210. doi:10.1038/nrmicro3215

4. Warren-Gash C, Forbes H, Breuer J. Varicella and herpes zoster vaccine development: lessons learned. *Expert Rev Vaccines*. 2017;16(12):1191-1201. doi:10.1080/14760584.2017.1394843

5. De Clercq E, Li G. Approved Antiviral Drugs over the Past 50 Years. *Clin Microbiol Rev*. 2016;29(3):695-747. doi:10.1128/CMR.00102-15

6. Wu Q, Rivailler P, Xu S, Xu W. Comparison of the Whole-Genome Sequence of an Oka Varicella Vaccine from China with Other Oka Vaccine Strains Reveals Sites Putatively Critical for Vaccine Efficacy. *J Virol*. 2019;93(9):e02281-18. doi:10.1128/JVI.02281-18

7. Sadaoka T, Depledge DP, Rajbhandari L, Breuer J, Venkatesan A, Cohen JI. A Variant Allele in Varicella-Zoster Virus Glycoprotein B Selected during Production of the Varicella Vaccine Contributes to Its Attenuation. *mBio*. 13(4):e01864-22. doi:10.1128/mbio.01864-22

8. Gershon AA, Gershon MD. Perspectives on Vaccines Against Varicella-Zoster Virus Infections. *Curr Top Microbiol Immunol*. 2010;342:359-372. doi:10.1007/82_2010_12

9. Seward JF, Watson BM, Peterson CL, et al. Varicella disease after introduction of varicella vaccine in the United States, 1995-2000. *JAMA*. 2002;287(5):606-611. doi:10.1001/jama.287.5.606

10. Cohen JI. Varicella-zoster vaccine virus: Evolution in action. *Proc Natl Acad Sci U S A*. 2007;104(1):7-8. doi:10.1073/pnas.0610016103

11. Willis ED, Woodward M, Brown E, et al. Herpes zoster vaccine live: A 10 year review of post-marketing safety experience. *Vaccine*. 2017;35(52):7231-7239. doi:10.1016/j.vaccine.2017.11.013

12. Quinlivan ML, Jensen NJ, Radford KW, Schmid DS. Novel Genetic Variation Identified at Fixed Loci in ORF62 of the Oka Varicella Vaccine and in a Case of Vaccine-Associated Herpes Zoster. *J Clin Microbiol*. 2012;50(5):1533. doi:10.1128/JCM.06630-11

13. Gomi Y, Sunamachi H, Mori Y, Nagaike K, Takahashi M, Yamanishi K. Comparison of the Complete DNA Sequences of the Oka Varicella Vaccine and Its Parental Virus. *J Virol*. 2002;76(22):11447-11459. doi:10.1128/JVI.76.22.11447-11459.2002

14. Khalil MI, Ruyechan WT, Hay J, Arvin A. Differential effects of Sp cellular transcription factors on viral promoter activation by varicella-zoster virus (VZV) IE62 protein. *Virology*. 2015;485:47-57. doi:10.1016/j.virol.2015.06.031

15. Kinchington PR, Fite K, Turse SE. Nuclear Accumulation of IE62, the Varicella-Zoster Virus (VZV) Major Transcriptional Regulatory Protein, Is Inhibited by Phosphorylation Mediated by the VZV Open Reading Frame 66 Protein Kinase. *J Virol*. 2000;74(5):2265-2277.

16. Sato B, Ito H, Hinchliffe S, Sommer MH, Zerboni L, Arvin AM. Mutational Analysis of Open Reading Frames 62 and 71, Encoding the Varicella-Zoster Virus Immediate-Early Transactivating Protein, IE62, and Effects on Replication In Vitro and in Skin Xenografts in the SCID-hu Mouse In Vivo. *J Virol*. 2003;77(10):5607-5620. doi:10.1128/JVI.77.10.5607-5620.2003

17. Depledge DP, Ouwendijk WJD, Sadaoka T, et al. A spliced latency-associated VZV transcript maps antisense to the viral transactivator gene 61. *Nat Commun*. 2018;9(1):1167. doi:10.1038/s41467-018-03569-2

18. Kennedy PGE, Montague P. Variable Gene Expression in Human Ganglia Latently Infected with Varicella-Zoster Virus. *Viruses*. 2022;14(6):1250. doi:10.3390/v14061250

19. Bose A, Teh MT, Mackenzie IC, Waseem A. Keratin K15 as a Biomarker of Epidermal Stem Cells. *Int J Mol Sci*. 2013;14(10):19385. doi:10.3390/ijms141019385

20. JOULAI VEIJOUYE S, YARI A, HEIDARI F, SAJEDI N, GHOROGHI MOGHANI F, NOBAKHT M. Bulge Region as a Putative Hair Follicle Stem Cells Niche: A Brief Review. *Iran J Public Health*. 2017;46(9):1167-1175.

21. Liu Y, Lyle S, Yang Z, Cotsarelis G. Keratin 15 promoter targets putative epithelial stem cells in the hair follicle bulge. *J Invest Dermatol*. 2003;121(5):963-968. doi:10.1046/j.1523-1747.2003.12600.x

22. Ito M, Liu Y, Yang Z, et al. Stem cells in the hair follicle bulge contribute to wound repair but not to homeostasis of the epidermis. *Nat Med*. 2005;11(12):1351-1354. doi:10.1038/nm1328

23. Jones M, Dry IR, Frampton D, et al. RNA-seq analysis of host and viral gene expression highlights interaction between varicella zoster virus and keratinocyte differentiation. *PLoS Pathog*. 2014;10(1):e1003896. doi:10.1371/journal.ppat.1003896

24. Garner E, Costanzo V. Studying the DNA damage response using in vitro model systems. *DNA Repair*. 2009;8(9):1025-1037. doi:10.1016/j.dnarep.2009.04.015

25. Yamamoto T, Ali MA, Liu X, Cohen JI. Activation of H2AX and ATM in varicella-zoster virus (VZV)-infected cells is associated with expression of specific VZV genes. *Virology*. 2014;452-453:52-58. doi:10.1016/j.virol.2013.12.039

26. Bonner WM, Redon CE, Dickey JS, et al. γH2AX and cancer. *Nat Rev Cancer*. 2008;8(12):957-967. doi:10.1038/nrc2523

27. Lloyd MG, Yee MB, Flot JS, et al. Development of Robust Varicella Zoster Virus Luciferase Reporter Viruses for In Vivo Monitoring of Virus Growth and Its Antiviral Inhibition in Culture, Skin, and Humanized Mice. *Viruses*. 2022;14(4):826. doi:10.3390/v14040826

28. Graybill C, Claypool DJ, Brinton JT, Levin MJ, Lee KS. Cytokines Produced in Response to Varicella-Zoster Virus Infection of ARPE-19 Cells Stimulate Lymphocyte Chemotaxis. *J Infect Dis*. 2017;216(8):1038-1047. doi:10.1093/infdis/jix426

29. Lloyd MG, Smith NA, Tighe M, et al. A Novel Human Skin Tissue Model To Study Varicella-Zoster Virus and Human Cytomegalovirus. *J Virol*. 2020;94(22):e01082-20. doi:10.1128/JVI.01082-20

30. Taylor SL, Moffat JF. Replication of Varicella-Zoster Virus in Human Skin Organ Culture. *J Virol*. 2005;79(17):11501-11506. doi:10.1128/JVI.79.17.11501-11506.2005

31. Leisenfelder SA, Moffat JF. Varicella-Zoster Virus Infection of Human Foreskin Fibroblast Cells Results in Atypical Cyclin Expression and Cyclin-Dependent Kinase Activity. *J Virol*. 2006;80(11):5577-5587. doi:10.1128/JVI.00163-06

32. Boice JD, Persson I, Brinton LA, et al. Breast cancer following breast reduction surgery in Sweden. *Plast Reconstr Surg*. 2000;106(4):755-762. doi:10.1097/00006534-200009040-00001

33. Lafouresse F, Groom JR. A Task Force Against Local Inflammation and Cancer: Lymphocyte Trafficking to and Within the Skin. *Front Immunol*. 2018;9. doi:10.3389/fimmu.2018.02454